Journal of Marine Science and Application
https://doi.org/10.1007/s11804-018-0042-4

RESEARCH ARTICLE

CFD Investigations of Ship Maneuvering in Waves Using naoe-FOAM-SJTU Solver

Jianhua Wang [1] · Decheng Wan [1]

Received: 26 March 2018 / Accepted: 2 June 2018

Abstract
Ship maneuvering in waves includes the performance of ship resistance, seakeeping, propulsion, and maneuverability. It is a complex hydrodynamic problem with the interaction of many factors. With the purpose of directly predicting the behavior of ship maneuvering in waves, a CFD solver named naoe-FOAM-SJTU is developed by the Computational Marine Hydrodynamics Lab (CMHL) in Shanghai Jiao Tong University. The solver is based on open source platform OpenFOAM and has introduced dynamic overset grid technology to handle complex ship hull-propeller-rudder motion system. Maneuvering control module based on feedback control mechanism is also developed to accurately simulate corresponding motion behavior of free running ship maneuver. Inlet boundary wavemaker and relaxation zone technique is used to generate desired waves. Based on the developed modules, unsteady Reynolds-averaged Navier-Stokes (RANS) computations are carried out for several validation cases of free running ship maneuver in waves including zigzag, turning circle, and course keeping maneuvers. The simulation results are compared with available benchmark data. Ship motions, trajectories, and other maneuvering parameters are consistent with available experimental data, which indicate that the present solver can be suitable and reliable in predicting the performance of ship maneuvering in waves. Flow visualizations, such as free surface elevation, wake flow, vortical structures, are presented to explain the hydrodynamic performance of ship maneuvering in waves. Large flow separation can be observed around propellers and rudders. It is concluded that RANS approach is not accurate enough for predicting ship maneuvering in waves with large flow separations and detached eddy simulation (DES) or large eddy simulation (LES) computations are required to improve the prediction accuracy.

Keywords Maneuvering in waves · Overset grid method · Hull-propeller-rudder interaction · OpenFOAM · naoe-FOAM-SJTU

1 Introduction

Ship maneuvering in waves is closely related to navigational safety. It includes the performance of ship resistance, seakeeping, propulsion, and maneuverability; thus, it is a very complex hydrodynamic problem with the interaction of many factors. Recently, the research of ship maneuvering in waves is becoming increasingly popular. Consequently, a specialist committee which is responsible for maneuvering in waves is established by the 28th International Towing Tank Conference (ITTC 2017). As one of the most difficult problems in the research of ship hydrodynamics, an accurate prediction approach for ship maneuvering in waves through either experimental or numerical method is still challenging.

Traditional experimental test in a conventional towing tank or wave basin still plays an important role in predicting the performance of seakeeping and ship maneuverability. However, conducting ship model tests of ship maneuvering in waves proposes a higher requirement of the measurement facility. So far, only a handful of institutes have the ability to do such complicated tests. The Iowa Institute of Hydraulic Research (IIHR) wave basin had done some free running ship

This study is financially supported by the National Natural Science Foundation of China (51809169, 51879159, 51490675, 11432009, 51579145), Chang Jiang Scholars Program (T2014099), Shanghai Excellent Academic Leaders Program (17XD1402300), Program for Professor of Special Appointment (Eastern Scholar) at Shanghai Institutions of Higher Learning (2013022), and Innovative Special Project of Numerical Tank of Ministry of Industry and Information Technology of China (2016-23/09).

✉ Decheng Wan
dcwan@sjtu.edu.cn

[1] State Key Laboratory of Ocean Engineering, School of Naval Architecture, Ocean and Civil Engineering, Collaborative Innovation Center for Advanced Ship and Deep-Sea Exploration, Shanghai Jiao Tong University, Shanghai 200240, China

Published online: 07 September 2018

maneuver tests in calm water and waves (Araki et al. 2012; Sanada et al. 2013). Sprenger et al. (2017) had done turning circle tests in Marintek wave basin within the SHOPERA project. However, the high cost of the experimental measurements and the complexity in local flow measurement still hold back its application.

So far, potential theory along with mathematical models has been extensively used in predicting the performance of ship maneuvering in waves. Seo and Kim (2011) applied a time-domain potential program to solve the wave-induced motion response, while the mean drift force and moment are considered in solving the Maneuvering Modeling Group (MMG) model. Their results show reasonable agreement but less accuracy. Zhang and Zou (2016) applied the 4 degrees of freedom MMG model to solve ship maneuvering motion and they determined the high frequency wave-induced motions by solving a linearized boundary value problem (BVP) in time domain. Subramanian and Beck (2015) and Paroka et al. (2017) applied a similar approach to conduct numerical predictions of ship maneuvering in waves. However, all the above predictions show considerable discrepancy compared with experimental data, which shows that the simplified method cannot accurately describe the maneuvering characters in waves.

Therefore, CFD methods are preferable in the predictions of ship maneuvering in waves. Direct CFD simulations are able to provide accurate prediction of hydrodynamic locals and specific local flow details since they can well resolve the complex flows around the hull and its appendages. Nevertheless, due to the high computational cost and complex numerical models, only few simulations of ship maneuvering in waves have been performed by CFD approach. Carrica et al. (2012) performed numerical simulations of ship maneuvering in waves by using a simplified body force propeller model and applied overset grid to handle the ship motions and rudder movement. Sigmund and el Moctar (2017) used sliding mesh to handle the complex ship hull-propeller-rudder motion system and simulated free running ship in waves. It shows the capability of CFD approach in directly simulating free running ship in waves. Shen and Korpus (2015) used dynamic overset grid technique and performed simulations of free running ship in head and quartering waves under course keeping control. Their results agreed well with the experimental data.

The objective of the present paper is to find out whether CFD approach along with dynamic overset grids and wave generation module is reliable in predicting ship maneuvering in waves. In the present study, the developed solver is applied to simulate several types of ship maneuvers in waves, such as zigzag maneuver, turning circle maneuver, and course keeping maneuver.

2 Numerical Approach

In the present work, CFD computations based on open source platform OpenFOAM are carried out to study the hydrodynamic performance of ship maneuvering in waves. During the calculation, the Reynolds-averaged Navier-Stokes (RANS) equations are solved for unsteady turbulent flows. A volume of fluid (VOF) approach with bounded compression technique is used (Berberović et al. 2009) to capture free surface. The shear stress transport (SST) turbulence model (Menter et al. 2003) is employed to model the turbulence features. In addition, wall functions are used to model the velocity gradient effects near the wall.

2.1 naoe-FOAM-SJTU Solver

Numerical computations are performed with the CFD solver naoe-FOAM-SJTU, which is developed on the open source platform OpenFOAM. The solver mainly includes dynamic overset grid module, 6 degrees of freedom (6DoF) module, and a numerical wave tank module (shown in section 2.2). Suggar++ (Noack et al. 2009) is utilized to calculate the domain connectivity information (DCI) for the overset grid interpolation. With the dynamic overset grid capability, a full 6DoF motion solver with a hierarchy of bodies is developed to handle the complex motion system of ship hull, propeller, and rudder. Detailed implementation of the overset grid module in OpenFOAM can be found in Shen et al. (2015). Maneuvering control module (shown in section 2.3) is also implemented in the solver to simulate standard ship maneuvers. So far, the solver has been extensively validated on large amount of ship hydrodynamic cases, e.g., ship resistance (Zha et al. 2014, 2015), seakeeping (Ye et al. 2012; Shen et al. 2014; Shen and Wan 2013, 2016; Wang and Wan 2016; Liu et al. 2018), propulsion (Shen et al. 2015; Wang et al. 2015), and maneuvering (Shen and Korpus 2015; Wang et al. 2016; Wang et al. 2018). More detailed information about the solver can be found in the references mentioned above.

2.2 Wave Generation and Absorption

There are two available wave generation approaches in naoe-FOAM-SJTU solver, namely, inlet boundary wavemaker and relaxation zone wavemaker.

2.2.1 Inlet Boundary Wavemaker

Inlet boundary condition is a typical approach to generate desired waves. In the present CFD solver, boundary conditions of $\boldsymbol{U}(u, v, w)$ in RANS equations are directly adopted as Dirichlet condition with specified wave theory. For the simulation of ship maneuvering in waves, only Airy wave

theory in deep water is adopted. The corresponding wave expressions are as follows:

$$\begin{cases} \zeta = a\cos(k{\cdot}x{-}\omega\, t{+}\theta) \\ u = a\omega\, \mathrm{e}^{kz}\cos(k{\cdot}x{-}\omega\, t{+}\theta) \\ v = a\omega\, \mathrm{e}^{kz}\cos\chi\cos(k{\cdot}x{-}\omega\, t{+}\theta) \\ w = a\omega\, \mathrm{e}^{kz}\sin\chi\cos(k{\cdot}x{-}\omega\, t{+}\theta) \end{cases} \quad (1)$$

where ζ is the wave elevation and u, v, and w represent the wave velocities in each direction; k is the wave number; and θ is the wave phase determined in the initial state of the incident waves. χ is the incident wave direction defined as the angle between the ship advancing direction and the wave direction. For instance, $\chi = 90$ is beam wave and $\chi = 180$ is following wave.

For the inlet boundary condition of volume fraction α, it needs special treatment when a boundary cell is divided by the wave elevation. The boundary condition of fraction α is obtained by the following expression.

$$\alpha = \begin{cases} 0, & \text{air} \\ \dfrac{S_W}{S_0}, & \text{free surface} \\ 1, & \text{water} \end{cases} \quad (2)$$

where S_0 is the total area of the cell face and S_W is the wetted face area. When the cell of the inlet boundary is totally below the transient wave elevation, in other words, the cell is located in water, then the value of α is 1. When a cell is totally in the region of air, then volume fraction is 0.

Apart from wave generation, the solver also has a wave absorption module, which is achieved by adding a source term in momentum equation. The source term only takes effects in a certain area of computational domain, usually extends to more than one wave length before outlet boundary. It is called sponge layer and is set ahead the outlet boundary with a certain length. Figure 1 illustrates the inlet boundary wave generation and absorption near outlet boundary. The source term in momentum equation is denoted as:

$$f_s(x) = \begin{cases} -\rho\alpha_s\left(\dfrac{x-x_s}{L_s}\right)^2(\boldsymbol{U}-\boldsymbol{U}_{\mathrm{ref}}) \\ 0 \end{cases} \quad (3)$$

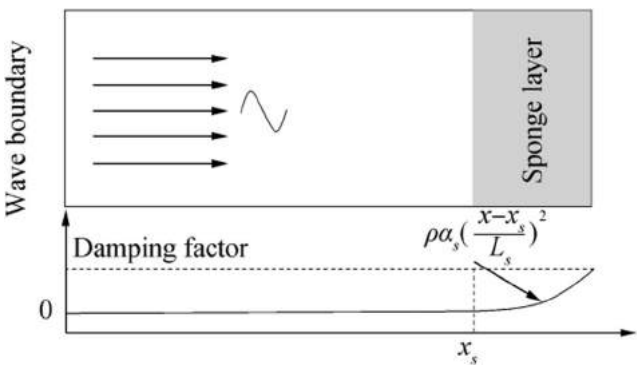

Fig. 1 Diagram of wave generation and absorption

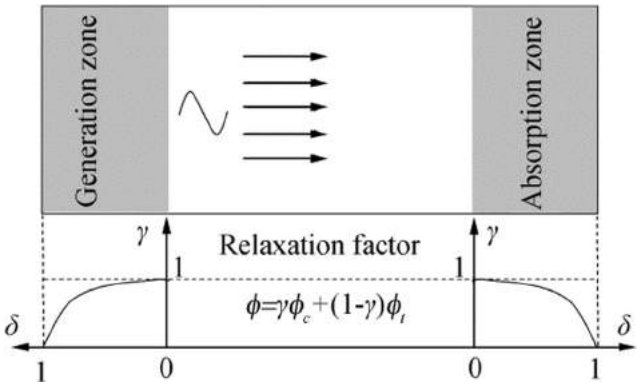

Fig. 2 Diagram of relaxation zone

where f_s is the source term, α_s is the damping coefficient, x_0 denotes the start position of wave damping zone, and L_s is the length of damping zone.

The distribution of the damping factor along the wave tank is depicted in Fig. 1. The inlet boundary wavemaker and the sponge layer type wave absorption method have been extensively validated in the previous work (Cao and Wan 2014, 2015, 2017; Shen and Wan 2016; Wang et al. 2017).

2.2.2 Relaxation Zone Wavemaker

For numerical simulation of ship maneuvering in waves with wide range, the computational domain, which consists of overset grids, is always treated as moving domain with the consideration of reducing the computational cost. Therefore, the inlet boundary wavemaker may be not appropriate since the boundary may deviate from its original position. In order to generate desired wave environment with the moving computational domain, the open source toolbox waves2foam (Jacobsen et al. 2012) is utilized in the present CFD solver. The methodology adopts the relaxation zones to avoid reflections of waves from outlet boundaries and further to avoid waves reflected internally in the computational domain to interfere with the wavemaker boundaries.

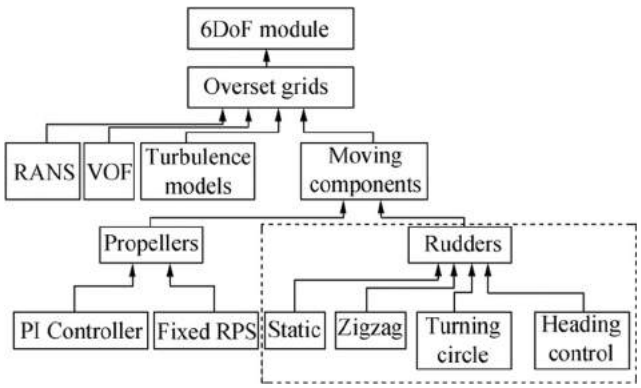

Fig. 3 Maneuvering control module in naoe-FOAM-SJTU

Fig. 4 Geometry model of ONR Tumblehome

The flow parameters ϕ in relaxation zone can be obtained by the following expression:

$$\phi = \gamma\phi_c + (1-\gamma)\phi_t \tag{4}$$

where flow parameters can be velocity $\boldsymbol{U}$ or volume of fraction α, and γ is relaxation factor. ϕ_c is the computed value and ϕ_t is the target value according to the corresponding wave theory. The schematic of the computational domain, wave generation zone, and absorption zone is shown in Fig. 2. The variation of relaxation factor γ is also depicted. The details of the relaxation technique can be found in Jacobsen et al. (2012). A frozen type relaxation zone is used in the present simulations so that the wave generation zone can move with the computational domain. This guarantees that the waves can propagate to the area around ship model no matter how the computational domain rotates or translates.

2.3 Maneuvering Control Module

In order to directly simulate free running ship maneuver, the movement of propellers and rudders need to be controlled according to the desired maneuvering motion. As mentioned in section 2.1, several control modules of standard maneuvers are implemented in naoe-FOAM-SJTU solver based on 6DoF module and feedback control mechanism. So far, typical maneuvers, such as zigzag maneuver, turning circle maneuver, and heading control maneuver, are developed to simulate corresponding ship maneuvering motion. Figure 3 illustrates the framework of 6DoF module associated with dynamic overset grids.

In the present solver, 6DoF motion is based on the Euler angle description and the equations are solved by a semi-implicit approach, where the solution is given by iterations to fulfill convergence. Overset grid module is implemented to handle complex motions of ship hull-propeller-rudder system. Propellers and rudders are inherited from the base class *Moving Components*, which can also derive to specific motion type based on class hierarchy. During the calculation, the overset grids belong to different motion levels according to motion control mechanism. The movements of propellers and rudders are children level motion to the ship hull motion, where the grids belonging to propeller and rudder are firstly updated and then together move with the 6DoF ship motion. Detailed information of the 6DoF motion module with a hierarchy of bodies can be found in Shen et al. (2015).

Table 1 Main particulars of ONR Tumblehome ship

Main particulars	Symbols	Model
Length of waterline/m	L_{WL}	3.147
Beam/m	B_{WL}	0.384
Draft/m	T	0.112
Displacement/kg	Δ	72.6
Wetted surface area/m^2	S_0	1.5
Block coefficient	C_B	0.535
Moment of inertia	K_{xx}/B	0.444
	K_{yy}/L_{WL}	0.246
Propeller diameter /m	D_P	0.1066
Rudder rate/((°)·s^{-1})		35.0

2.3.1 Course Keeping Maneuver

The course keeping maneuver module is developed to extend the capability of CFD solver naoe-FOAM-SJTU (section 2.1) in simulating free running ship under course keeping control. The rudder is controlled by a PID feedback controller, where the rudder is executed according to the deviation of yaw angle from target heading angle. The control mechanism is as follows:

$$\delta(t) = K_P e(t) + K_I \int_0^t e\left(t'\right)\mathrm{d}t' + K_D \frac{\mathrm{d}e(t)}{\mathrm{d}t} \tag{5}$$

where K_P, K_I, and K_D are proportional, integral, and derivative coefficients, respectively. $e(t)$ is the deviation between

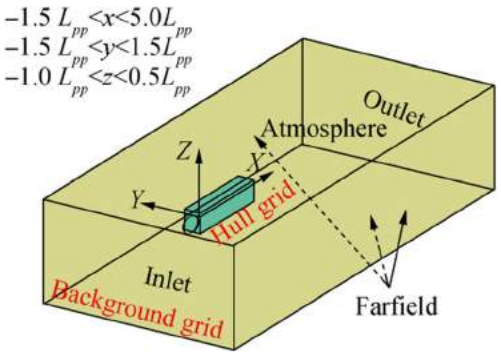

Fig. 5 Computational domain

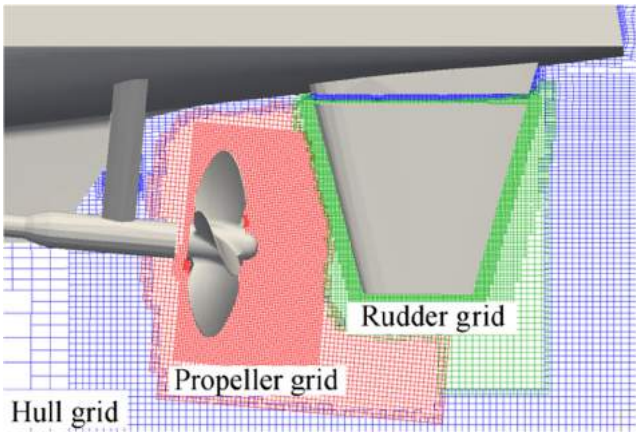

Fig. 6 Local grid distribution

instantaneous yaw angle $\psi(t)$ and target yaw angle ψ_t. $e(t)$ is denoted by:

$$e(t) = \psi(t) - \psi_t \tag{6}$$

The coefficients of PID controller are following the setup of experimental test or sea trial.

2.3.2 Zigzag Maneuver

Zigzag maneuver is one of the typical approaches to access ship maneuverability. For a standard zigzag maneuver, the ship is moving forward with nominal constant speed and the rudder is executed to a specified maximum rudder angle at the maximum rudder rate. Then, the ship responses with a turning motion due to the rudder deflection. When the heading angle reaches check heading angle, the rudder is then turned at maximum rudder rate in the opposite direction until it reaches the specified rudder angle.

The zigzag maneuver is inherited from base class "rudder," which is a derived class of moving component as shown in Fig. 3. For a standard 10/10 zigzag maneuver, the rudder deflection $\delta(t)$ follows the feedback control mechanism:

$$\delta(t) = \begin{cases} \min(kt, 10), & t_1 \le t \le t_2 \\ \max(-kt, -10), & t_2 \le t \le t_3 \\ \min(kt, 10), & t_3 \le t \le t_4 \end{cases} \tag{7}$$

where $\delta(t)$ is the rudder angle, which is positive when the rudder turns to the starboard side; k is the maximum rudder rate; and t_i is the ith time for rudder execution.

2.3.3 Turning Circle Maneuver

Turning ability is very important for a navigational ship and it can be accessed by the performance of turning circle maneuver. The implementation of turning circle maneuver is easy to accomplish based on the code structure and similar with zigzag maneuver. The control mechanism is according to the

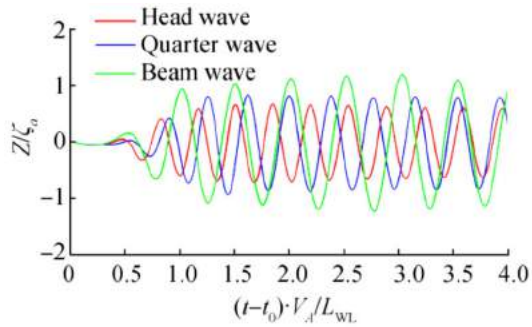

(a) Heave motion

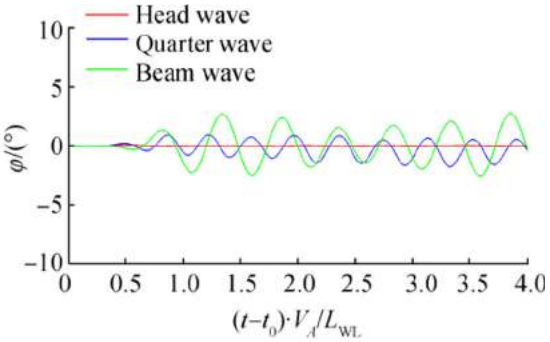

(c) Roll motion

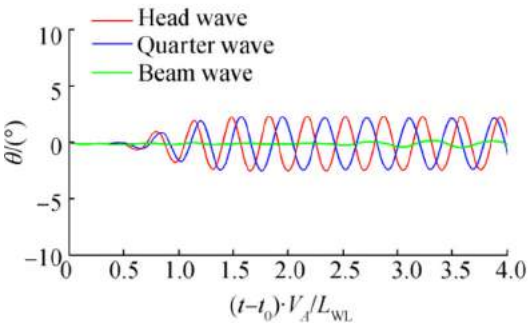

(b) Pitch motion

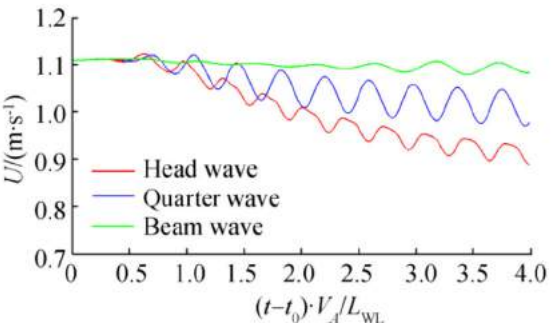

(d) Ship speed

Fig. 7 Comparison of ship motions and ship speed in different waves

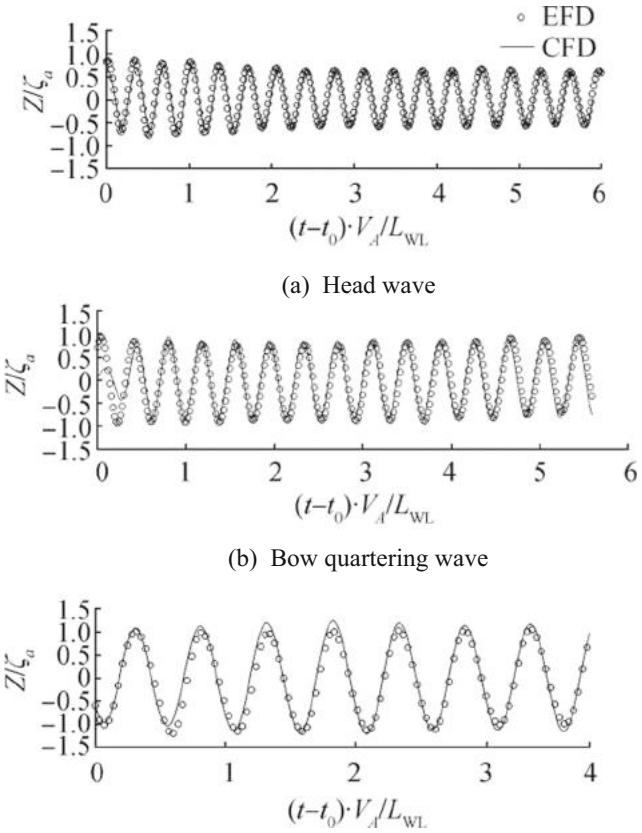

(a) Head wave

(b) Bow quartering wave

(c) Beam wave

Fig. 8 Comparison of heave motion with experiment

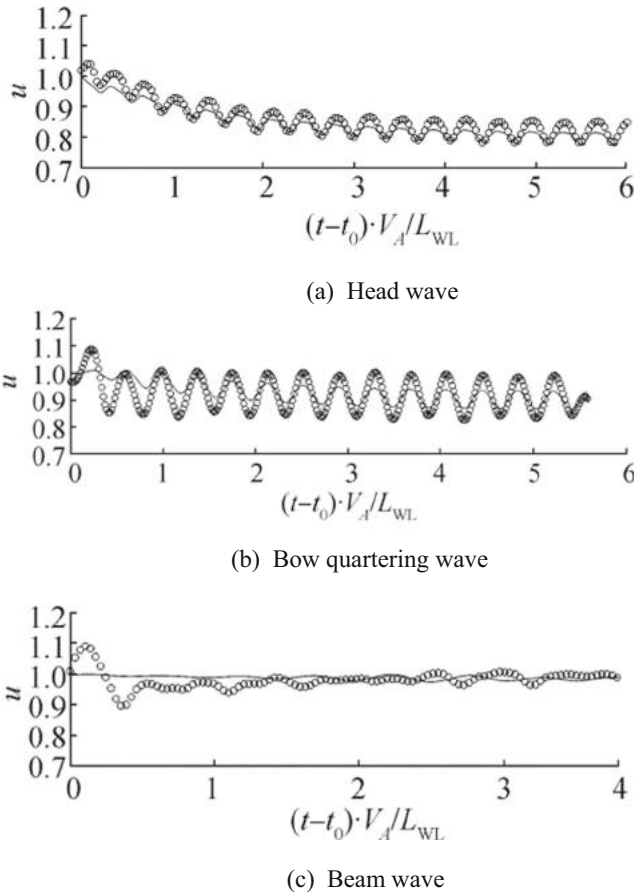

(a) Head wave

(b) Bow quartering wave

(c) Beam wave

Fig. 9 Comparison of ship speed with experiment

specified turning control parameters. For a turning maneuver with a 35° starboard case, the rudder deflection $\delta(t)$ follows the expressions:

$$\delta(t) = \begin{cases} \max(0, kt), & \delta \le 35 \\ 35 \\ \max\left(35 - k\left(t - t_p\right), 0\right), & t \ge t_p \end{cases} \tag{8}$$

where k is the maximum rudder rate and t_p is pull out angle used to stop turning.

3 Course Keeping Maneuver

The ship model ONR Tumblehome used as a benchmark ship model in Tokyo 2015 CFD workshop in ship hydrodynamics is applied for the numerical simulations of ship maneuvering in waves under course keeping control. EFD results are also available for the course keeping tests. The geometry model of ONR Tumblehome is shown in Fig. 4, and the principle geometric characteristics both in model scale and full scale are listed in Table 1.

In order to directly simulate the twin-screw fully appended ship, the computational domain is divided into six parts. The computational domain and boundary conditions are shown in Fig. 5 and the local grid distribution is shown in Fig. 6. The $Y+$ is around 60 for the hull grids and the total grid number is 7.11 million.

According to the model tests, the rudder deflection adopts an auto-pilot control mechanism (PI Controller) to accomplish the course keeping control, where the integral and derivative coefficients in Eq. (5) are 0 and the proportional coefficient is 1. The fully appended ship is set to advance at model point (8.819RPS) with full 6DoF motion in both calm water and regular waves. The target ship speed is $U_0 = 1.11$ m/s ($Fr = 0.20$) with the wave condition of $\lambda/L_{WL} = 1.0$, $H/\lambda = 0.02$, where λ is the wave length and H is the wave height. Three incident waves, i.e., head wave, bow quartering wave, and beam wave, are considered in the simulation. Inlet boundary wavemaker is used to generate desired wave environment. Main focus is put on the wave direction effects on ship motions and the capability of CFD methods in predicting course keeping maneuver.

The computations are carried out on a HPC cluster (IBM nx360M4) in the Computational Marine Hydrodynamics

Lab (CMHL), Shanghai Jiao Tong University. Forty processors are assigned to calculate the course keeping maneuver in different incident waves, in which 38 processors are for the flow calculation and the other 2 processors are used for DCI computation by Suggar++. The time step was set to $\Delta t = 0.0005$s in order to resolve the transient flow due to the rotating propeller, which corresponds to approximately 1.5° of propeller rotation per time step, and the resultant Courant number is around 0.1. All the simulations are started from the previous self-propulsion steady state. Time to complete the computation was approximately 225 wall clock hours and 8979 CPU hours with about 38000 time steps.

Similar to most researches regarding CFD simulations of free running ship maneuver, the verification study such as grid convergence study is not conducted in this paper considering the high computational cost. The grid refinement will strongly affect the quality of overlapping grids, especially for the complex hull-propeller-rudder system, where the gaps between each component are very small. For simpler geometries, such as the cases with single hull, open water computations, good grid convergence has been obtained (Shen et al. 2015; Wang et al. 2018) by using the same CFD solver naoe-FOAM-SJTU. Thus, in this work, main focuses have been placed on the applications for various ship maneuvers by comparing with available experimental results.

In this section, the CFD and EFD results for ship motions and velocities are in non-dimensional format. Heave motion Z is normalized by wave amplitude ζ_a. Ship speed u is non-dimensionalized by target advancing speed V_A. Time axis is normalized by initial time when ship begins to move t_0, target ship speed V_A, and ship length L_{WL}.

Figure 7 shows the comparisons of predicted ship motions and instantaneous ship speed under different incident waves. It is obvious that wave-induced heave motions are severe in all three heading waves. Pitch motion in beam waves is rather small since the disturbance is mostly taken effect on transverse direction, which lead to the largest wave-induced roll motion

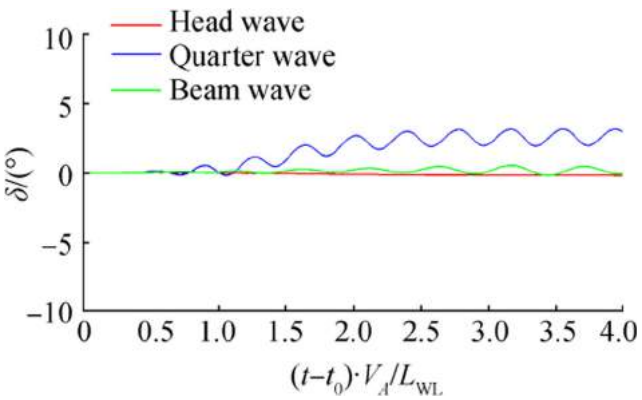

Fig. 10 Comparison of rudder deflection in different waves

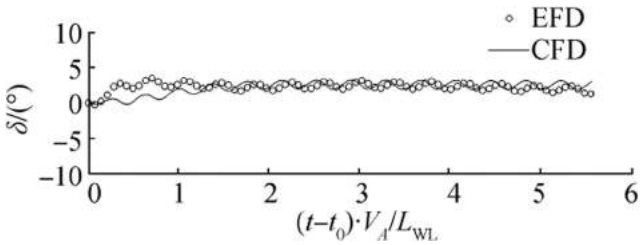

Fig. 11 Comparison of rudder deflection with experiment

in beam waves as shown in Fig. 8c. Apart from the ship motions, ship speeds also show much difference in different heading waves. Head wave meets the largest speed loss, which can be as large as 17%. The speed loss of bow quartering wave and beam wave is 9% and 2%, respectively. The predicted results are also compared with the available experimental data provided by Tokyo 2015 CFD Workshop. Figures 8 and 9 show the comparison of predicted heave motion and ship instantaneous speed with experimental data. Though some discrepancies can be observed, the present CFD results show an overall agreement with the experimental measurements.

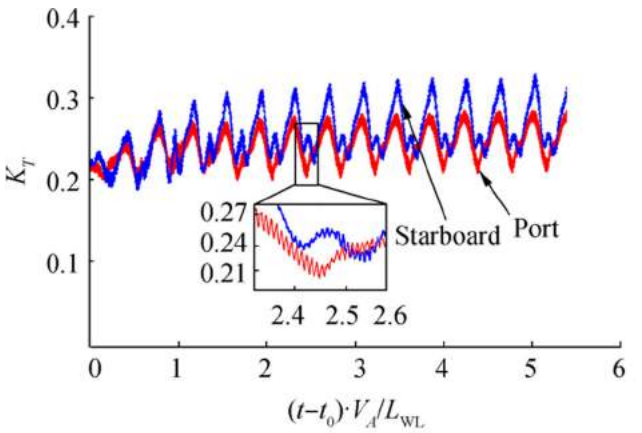

(a) K_T

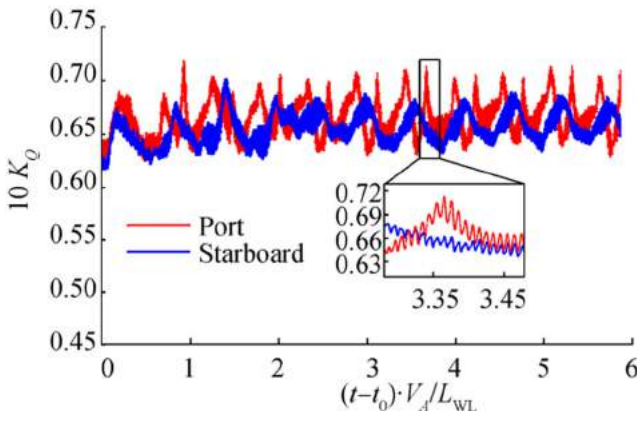

(b) $10K_Q$

Fig. 12 Propulsion performance in bow quartering waves. **a** K_T; **b** $10K_Q$

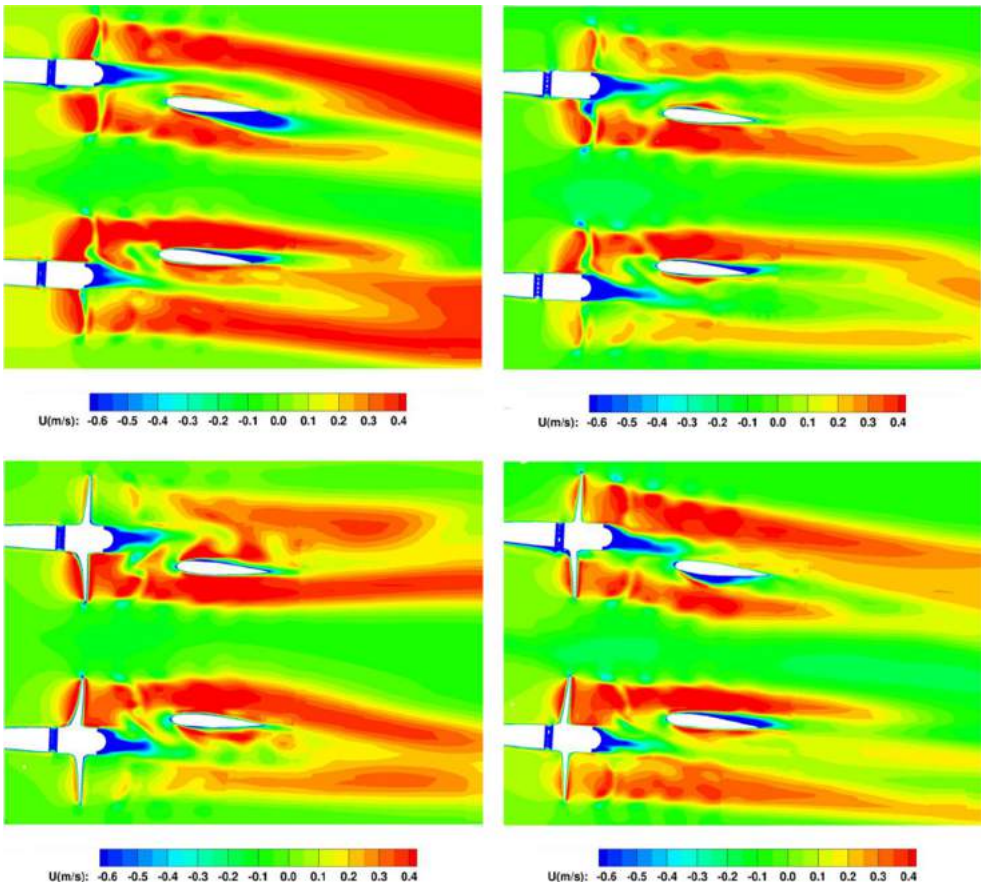

Fig. 13 Wake flow around twin propellers and rudders in one wave period

The rudder deflection in different waves is shown in Fig. 10. It is obvious that the rudder execution in bow quartering waves is very important to achieve target heading angle. The maximum rudder angle is 3.2°. However, for beam wave and head wave condition, the rudder deviation is rather small compared with the bow quartering wave.

The predicted rudder angle is also compared with the experimental results as shown in Fig. 11. The present CFD results can give an overall estimation of the rudder execution during free running ship in waves under course keeping control, which indicates that the developed course keeping maneuver module is reliable.

CFD simulation can not only give the prediction of ship motions, but also can present propulsion performance as well as the detailed flow information, which make it more attractive than the traditional experiment. The predicted propulsion coefficients, i.e., K_T and $10K_Q$, in bow quartering waves are presented in Fig. 12. Both port and starboard thrust and torque

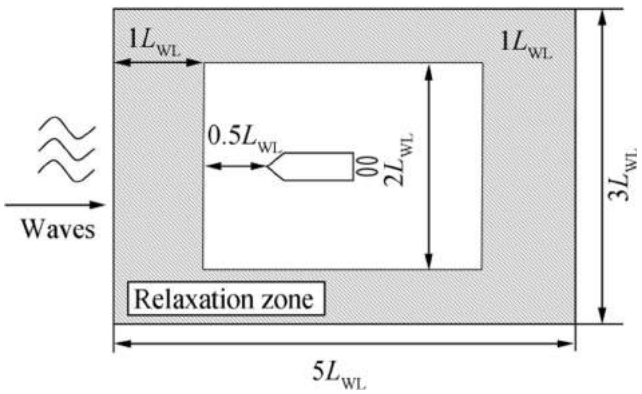

Fig. 14 Computational domain and wave generation zone for zigzag maneuver simulation

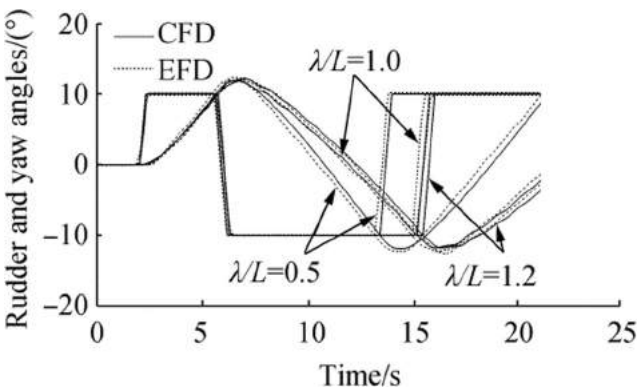

Fig. 15 Comparisons of time histories of yaw angle and rudder execution for zigzag maneuver in waves

Table 2 Comparison of zigzag parameters in different waves

Parameters	$\lambda/L = 0.5$		$\lambda/L = 1.0$		$\lambda/L = 1.2$	
	EFD	CFD	EFD	CFD	EFD	CFD
1st OSA/(°)	2.20	1.94	2.08	1.83	2.13	1.81
2nd OSA/(°)	2.21	1.86	2.54	2.15	2.14	1.86
Period/s	15.67	15.76	19.77	20.04	19.29	19.43

Table 3 Comparison of quantities of ship motions and speed in different waves

Parameters	$\lambda/L = 0.5$	$\lambda/L = 1.0$	$\lambda/L = 1.2$
$Roll_{min}$/(°)	−2.85	−2.63	−3.52
$Roll_{max}$/(°)	2.91	2.80	2.74
Heave/($\times 10^{-2}$m)	0.18	1.82	2.39
Pitch/(°)	0.11	2.29	2.87
Speed/(m·s^{-1})	1.04	0.87	0.89

coefficients show strong asymmetry behavior. The thrust coefficient of the starboard propeller is larger than that of the port side propeller for almost all the time. This can be explained by the different inflow for twin propellers in bow quartering waves and this can be better understood from the flow visualizations shown in Fig. 13. The torque coefficients also show difference for both side propellers. In addition, high frequency fluctuations in thrust and torque coefficients that correlate to the blade passage frequency are also observed in the predicted results shown in the partial enlarged view.

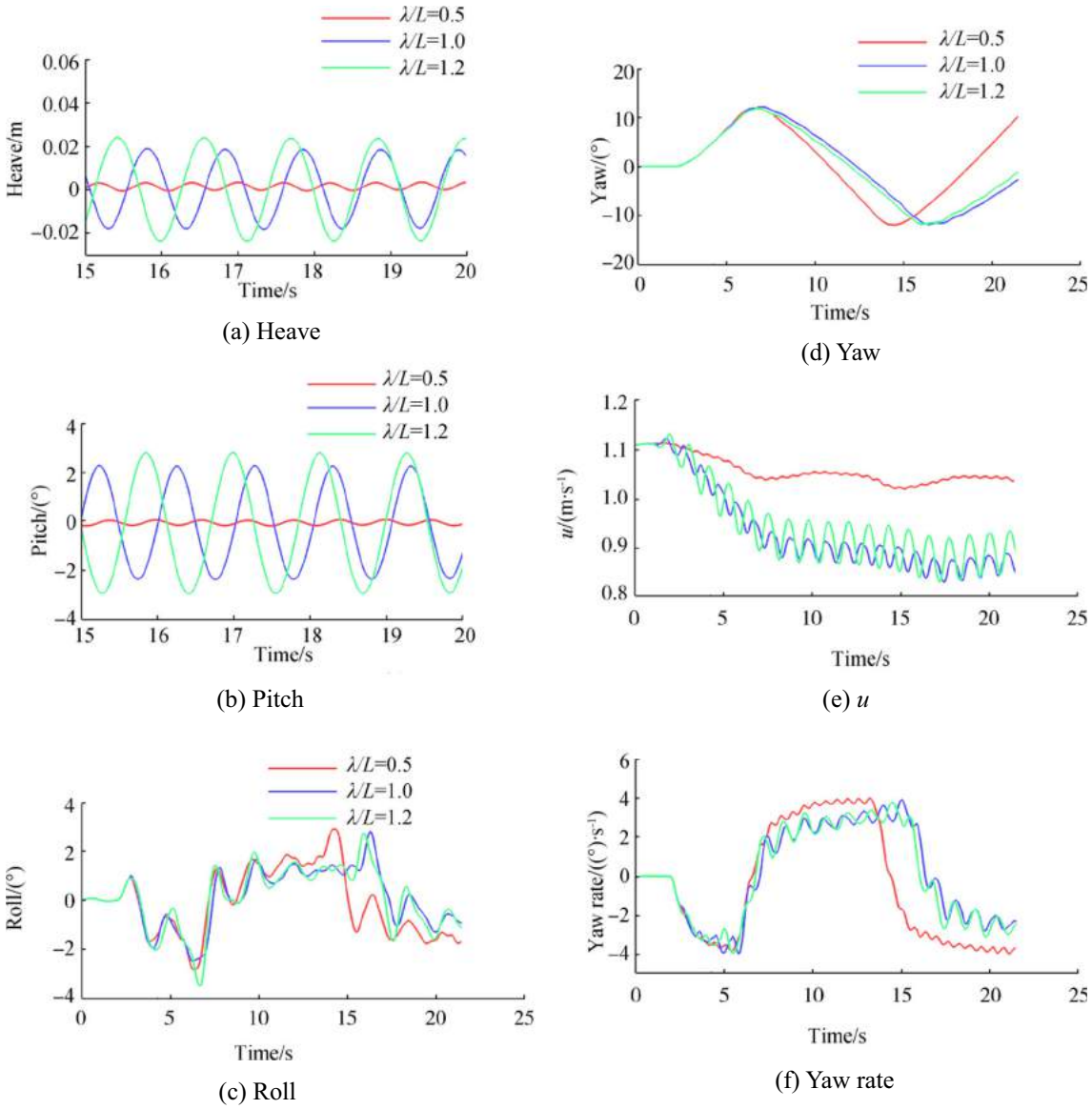

Fig. 16 Comparisons of ship motions in different waves

4 Zigzag Maneuver

In this section, the simulation of free running zigzag maneuver in waves is conducted using the developed zigzag maneuver control module. Twin-screw ONR Tumblehome ship model with standard 10/10 zigzag maneuver is simulated to investigate the hydrodynamic performance of ship maneuvering in waves. Computational setup is similar with the previous course keeping maneuver. Three incident waves with different wave lengths are considered, i.e., $\lambda/L_{WL} = 0.5$, $\lambda/L_{WL} = 1.0$, and $\lambda/L_{WL} = 1.2$, with same wave steepness of $H/\lambda = 0.02$. Different from the course keeping maneuver, the maneuvering motion can extend to a very large range for the zigzag maneuver. Thus, the relaxation zone type wavemaker is used to generate wave environment in moving computational domain. The diagram of the computational domain and wave generation zone is depicted in Fig. 14.

Main focuses of this part have been placed on the wave length effects on free running zigzag maneuver. More discussions for the wave height influences and calm water comparison can be found in Wang et al. (2018). The analysis will proceed with the motion performances, hydrodynamic forces, and detailed flow visualizations. The calculations are carried out at CMHL in Shanghai Jiao Tong University. It costs approximately 347 h of clock time with about 39 000 time steps to complete the computations of zigzag maneuver in waves.

Figure 15 shows the simulation results of the time histories of ship yaw angle and rudder execution during 10/10 zigzag maneuver in three different waves. The CFD results are consistent with the experiment measurements for all wave conditions, though some discrepancies are observed for both yaw and rudder angle. In general, the predicted period to complete one zigzag turn is slightly overestimated for all the three wave conditions. Detailed quantities, such as overshoot angles (OSA) and period of a standard zigzag maneuver, are listed in Table 2. Both first (1st) and second (2nd) overshoot angles are underestimated to some extent, while the total trend matches very well with the measurements. The parameters of period to complete one zigzag turn are accurately predicted with an error varying from 0.56% to 1.54%.

The comparison between time histories of ship motions and velocities in different waves is shown in Fig. 16. The heave and pitch motions under different wave conditions are localized to a smaller time scale with the purpose of better understanding the wave length effects on the ship performance. In order to characterize the wave effects on the free running ship maneuvers, the Fourier series (FS) (Shen and Wan 2013; Tezdogan et al. 2015) is used to analyze the ship motions and velocities due to waves. The mean amplitude of the oscillations of heave and pitch motions is quantified by the 1st harmonic FS term. Mean ship speed is represented by 0th harmonic FS term. Roll motions are quantified by the maximum and minimum value. The comparison of quantities is

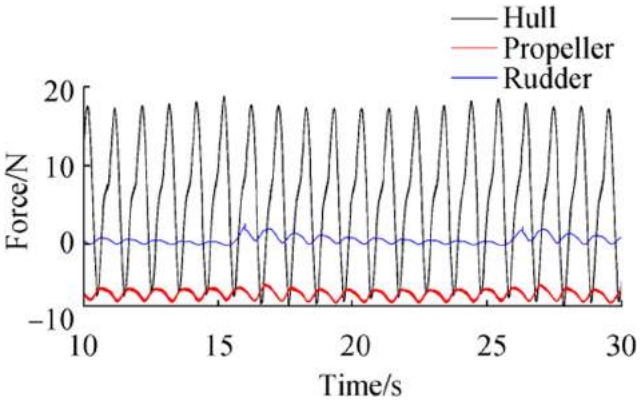

Fig. 17 Comparison of hull, propeller, and rudder forces

listed in Table 3. Heave and pitch motions show strong relations with the wave lengths, where the amplitudes increase with the increasing of wave length. Furthermore, the heave and pitch motions are significantly enlarged when the wave length is around one ship length. The amplitude of roll motions in all three waves are around 2.8°, while the minimum roll motion in waves of $\lambda/L_{WL} = 1.2$ is much larger with a value of 3.52°. The speed loss is a main character for ship advancing in waves and it can be obtained by the ship instantaneous speed. The speed loss can be obtained by the mean value of the speed characterized by the 0th harmonic term of FS term. The speed loss in waves of $\lambda/L_{WL} = 0.5$, $\lambda/L_{WL} = 1.0$, and $\lambda/L_{WL} = 1.2$ is 6.76%, 21.85%, and 19.65%, respectively.

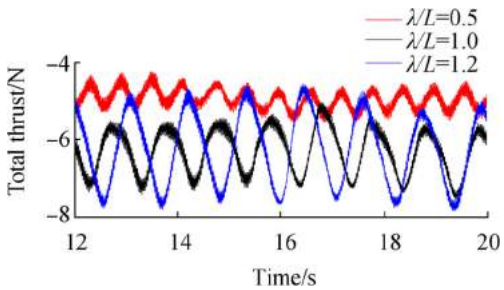

(a) Total thrust

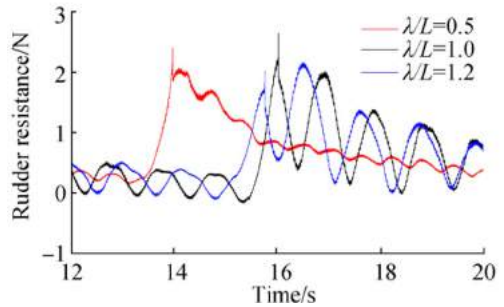

(b) Rudder resistance

Fig. 18 Comparisons of total thrust and rudder resistance in different waves

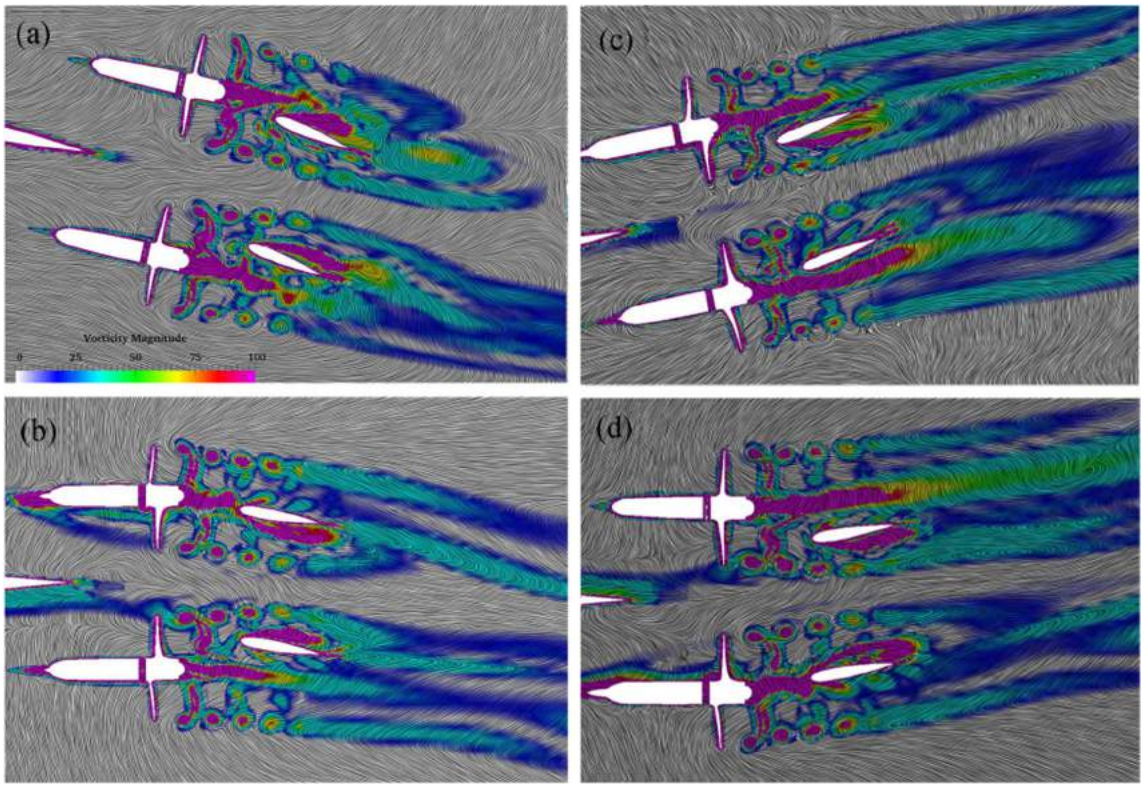

Fig. 19 Horizontal section of wake region around twin propellers and rudders during one zigzag period (**a** and **c** show the time of maximum and minimum yaw, **b** and **d** correspond to zero yaw, respectively)

Hydrodynamic forces acting on ship geometry can directly reflect the motion behavior during the zigzag maneuver in waves. Figure 17 presents the longitudinal forces on ship hull, propeller, and rudder in waves of $\lambda/L_{WL} = 1.0$, where the propeller force or rudder force are the resultant force on the twin propeller or the twin rudder. As can be seen from the figure, the ship resistance takes the main part of the total resistance, and the large fluctuations lead to the oscillations of ship speeds shown in Fig. 16.

Figure 18 presents the total thrust and rudder resistance in different waves. It is obvious that the fluctuation amplitude of total thrust and rudder resistance is larger when the wave length increases. The rudder resistance experiences transition when the rudder executes due to the maneuvering motion. It can be noticed that longest wave length case meets the largest fluctuation of total thrust and rudder resistance. The mean

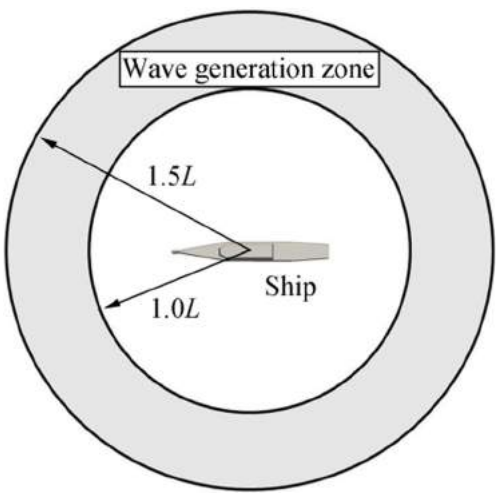

Fig. 20 Diagram of wave generation zone

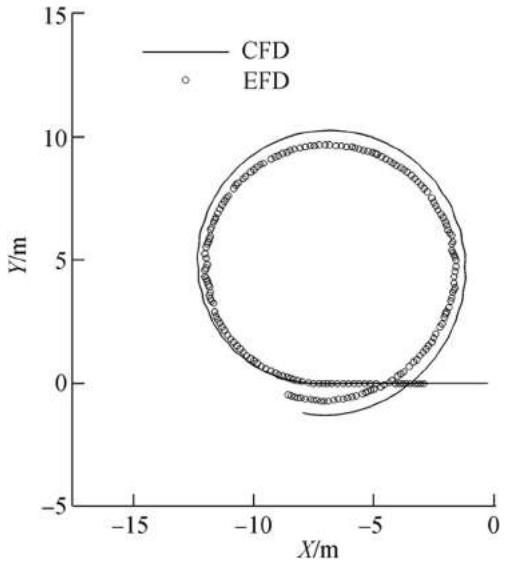

Fig. 21 Comparison of trajectory of turning circle maneuver in waves

value of the ship resistance and total thrust for waves of λ/L = 1.0 is almost the same with waves of λ/L = 1.2, while the mean amplitude of fluctuations obtained by the 1st harmonic FS term can be enlarged by 80.5% and 66.1%, respectively, in the longer wave case.

Apart from the ship motions and hydrodynamic forces of ship maneuvering in waves, the flow visualization is also presented to show the detailed flow during the maneuvering motion. Figure 19 illustrates the wake field around twin propellers and rudders in one zigzag turn. Figure 19a, c shows maximum and minimum yaw; Fig. 19b, d is zero yaw. Flow separation of twin rudders is evident and it is strongly affected by the hub vortices of the rotating propellers. At time instant Fig. 19a, c, the hub vortices of starboard side are disturbed by the aligned rudder and cause violent flows around the rudder. On the contrary, the port side hub vortices are significantly affected by the rudder at time instant Fig. 19b, d. Furthermore, the existence of the rudders can even affect the tip vortices, which can be clearly seen for the port side vortices at time instant Fig. 19a, b. The evident flow separations for the twin rudders and its encountering complex flows can play an important role for the ship maneuver in waves. Thus, the present RANS approach may be not accurate enough in predicting such kind of flow phenomena and it is one of the reasons that lead to the inaccuracy in predicting the trajectory and ship motions as shown in Fig. 15 and Table 2.

5 Turning Circle Maneuver

In this section, numerical simulation for standard turning circle maneuver with 35° rudder deflection turning to starboard is carried out. The ship model is the same with course keeping and zigzag maneuver simulations. The initial ship speed is U = 1.11 m/s with corresponding Froude number of 0.20. During the simulation, the rotational speed of propellers is set fixed with constant value of 8.819 RPS. The rudder is controlled regarding the standard turning circle maneuver shown in Eq. (8). The incident wave parameters follow the experimental setup (Elshiekh 2014; Sanada et al. 2013), where the wave length equals ship length ($\lambda = L_{WL}$) and wave steepness (H/λ) is 0.02.

To simulate turning circle maneuver in waves, a circular ring form relaxation zone is used to generate desired wave environment. Figure 20 demonstrates the computational domain and the wave generation zone. During the simulations, the wave generation zone is fixed with the moving computational domain, and therefore, the waves can propagate to the inner zone.

The initial flow state of the turning circle maneuver computation is from the stable state of self-propulsion condition, then the ship model is released in 6 degrees of freedom with specified rudder control to achieve the turning circle maneuver motion. Since the turning period is relatively longer, the computation expense is very high. It costs approximately 1206 h of clock time with about 155 000 time steps to complete the computation in waves.

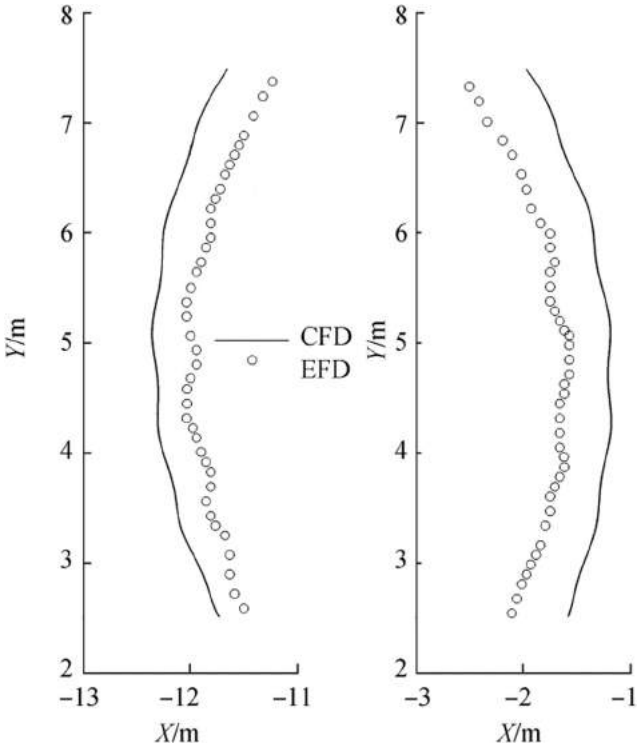

Fig. 22 Local comparison of turning trajectory

Figure 21 shows the predicted trajectory of turning circle maneuver in waves compared with the experimental measurements. The CFD results of trajectory is a bit larger than that of experiment. It may be caused by two factors. First is that the rudder geometry is modified in the computation to get enough interpolation cells. Consequently, the effective rudder area is smaller, which leads to the insufficient turning ability. Another reason is the present RANS approach, which is not accurate enough to resolve the large flow separation with such considerable rudder angle.

Through the comparison, we can see that there are obvious oscillations for the trajectory with the heading angle change around 90° and 270°. Figure 22 gives a local view of the

Table 4 Comparison of main parameters of turning circle maneuver

Parameters	CFD	EFD (Elshiekh 2014)	Error/ %
Advance A_D/m	6.9171	6.9978	− 1.15
Transfer T_R/m	4.1063	3.8797	5.84
T_{90}/s	12.2822	11.5700	6.15
Tactical T_A/m	10.1838	9.6213	5.85
T_{180}/s	24.5894	22.4100	9.72
Turning T_D/m	10.2807	9.6464	6.57

comparison for trajectory when encountering beam wave conditions. From the figure, we can see that despite the deviation from the experimental data, the wave effects on the trajectory can be captured well using the present approach.

The predicted main parameters of turning circle maneuver, i.e., advance, transfer, tactical diameter, turning diameter as well as time to 90°/180° heading change, and their comparisons with available experimental data, are shown in Table 4. It should be noted that the time has been shifted to the same rudder execution time so as to give the correct comparison of when to achieve 90° or 180° heading change. The predicted results show good agreement with the experiment measurement performed at IIHR wave basin (Elshiekh 2014; Sanada et al. 2014), with error up to 10%. It shows that the present numerical approach can give an overall evaluation of the maneuvering behavior in waves.

Figure 23 presents the time histories of ship motions, i.e., heave, pitch, roll, as well as ship instantaneous speed. Ship heave, pitch, and roll motions experience significant wave-induced motions. In addition, low frequency motion due to maneuvering motion can also be noticed. Maximum pitch angle during the turning circle motion is around 2.5° and the roll motion varies from −4.4° to 8°. For the curve of ship speed, we can see that the speed loss is significant during the turning circle maneuver, where the speed loss can be as large as 40%. The ship speed first drops due to the incident waves and the rudder deflection, then the ship speed keeps a relatively average loss of 30% at the steady turning circle stage.

Figure 24 shows the time histories of thrust and torque of twin propellers during the turning circle maneuver in waves. At the beginning, the ship is advancing straight forward and the thrust variation for the port and starboard side is almost the same, and the torque variations are symmetric. As soon as the rudder executes, both thrust and torque become asymmetry. The curves show alternating behavior for the amplitude of the fluctuations for the windward and leeward side propulsion forces. The very high frequency fluctuations due to the rotating propellers pass through the flow field can be observed from the enlarged view.

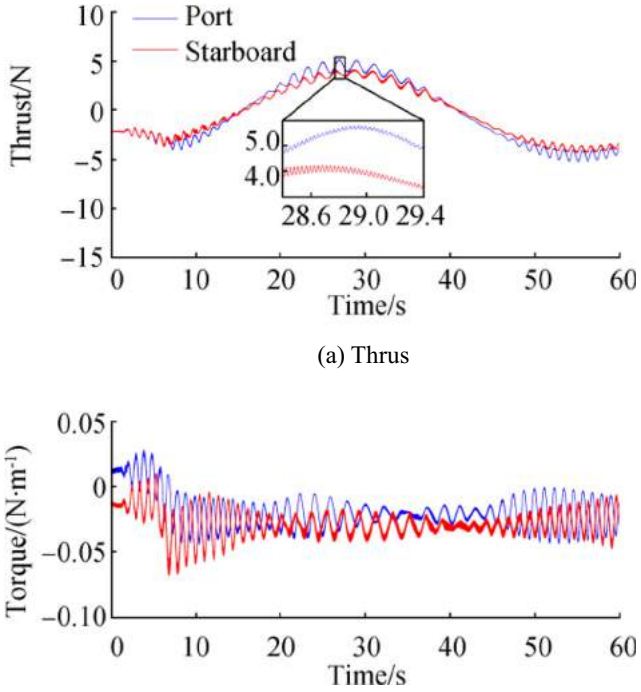

(a) Thrus

(b) Torque

Fig. 24 Time histories of thrust and torque during turning circle maneuver in waves

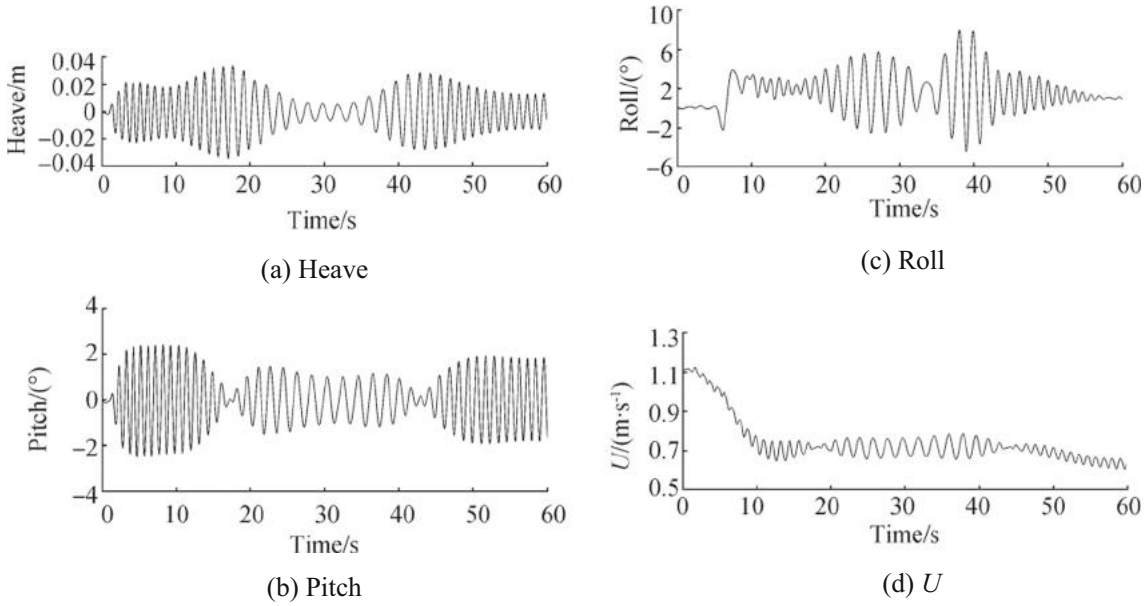

(a) Heave

(c) Roll

(b) Pitch

(d) U

Fig. 23 Time histories of heave, pitch, roll, and ship speed during turning circle maneuver in waves

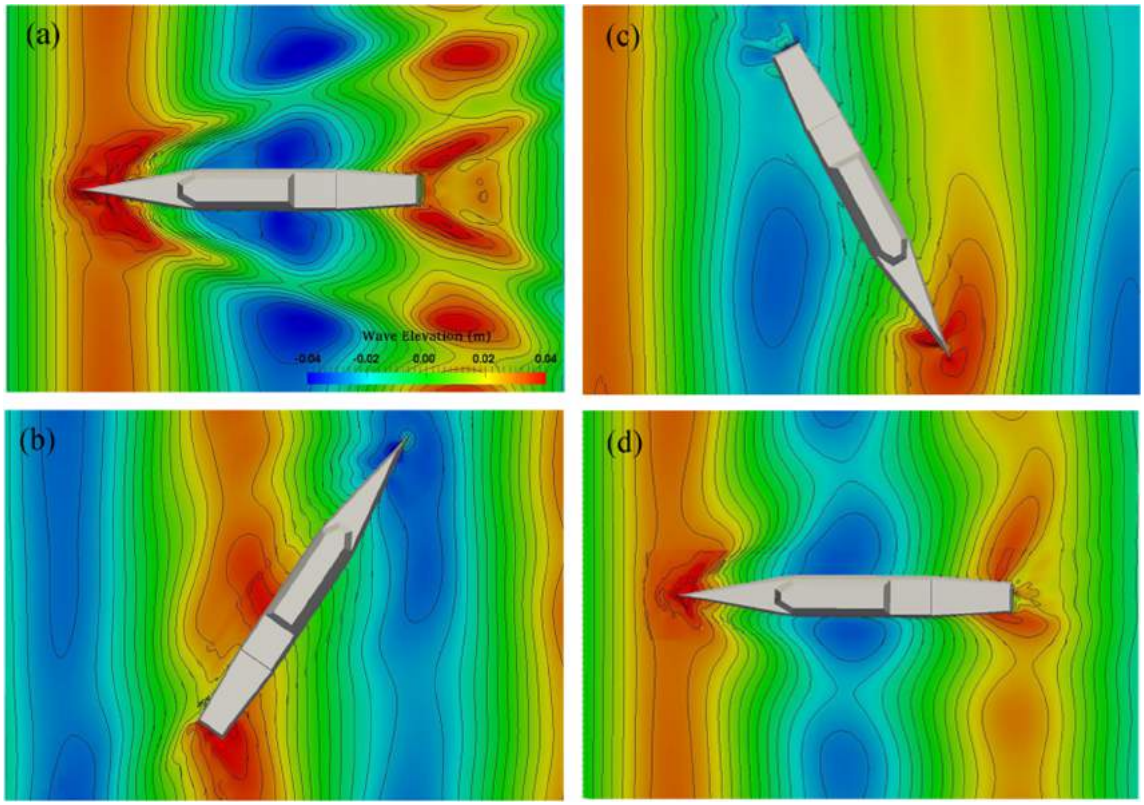

Fig. 25 Free surface elevation during turning circle maneuver in waves (**a**–**d** correspond to heading change of 0, 120, 240 and 360, respectively)

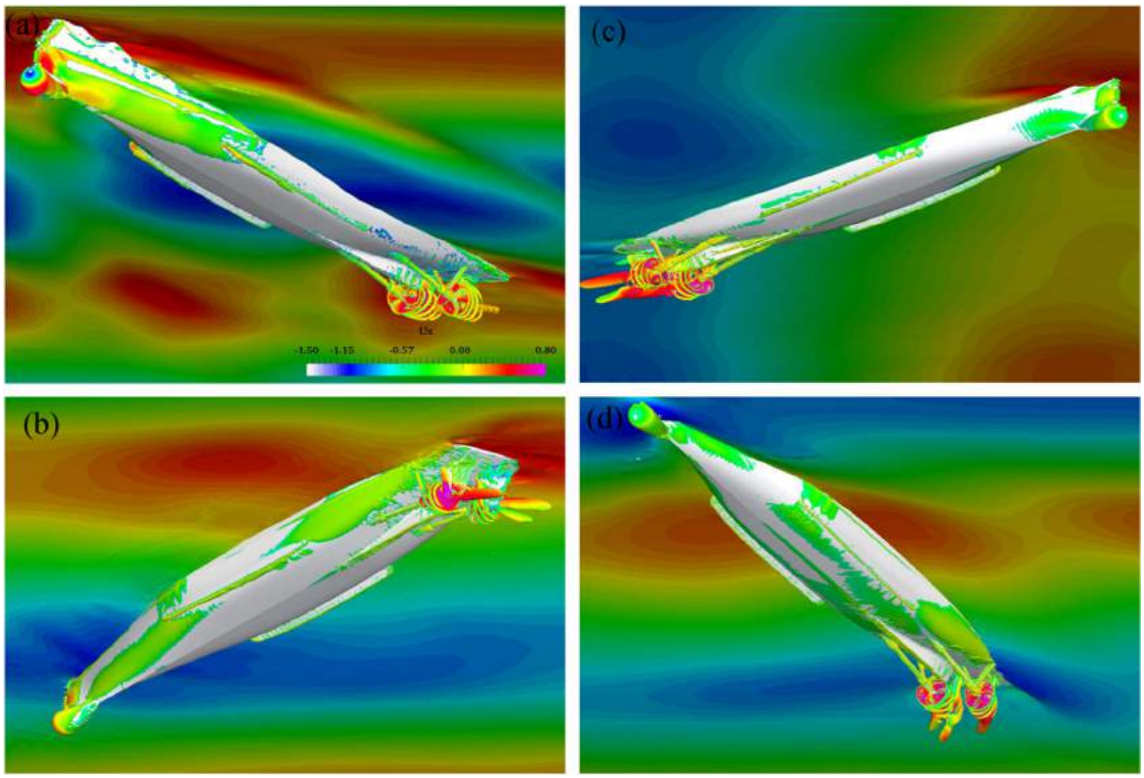

Fig. 26 Vortical structures around ship hull, twin propellers and rudders during turning circle maneuver in waves (**a**–**d** correspond to heading of 0, 120, 240 and 360, respectively)

Figure 25 presents four snapshots of free surface elevation during one period of turning circle maneuver in waves, corresponding to heading angle of 0°, 120°, 240°, and 360°. At time instant Fig. 25a, the wave pattern is symmetric with the fact that the ship is just advancing straight forward. However, when the ship undergoes turning condition, the wave distribution around ship hull is strongly different. As can be seen in time instants Fig. 25b–d, the bow wave and stern wave show much asymmetric. This phenomenon will further cause the pressure difference on both side of ship hull.

Vortical structures around ship hull, twin propellers, and rudders are depicted in Fig. 26 with the same time instants in Fig. 25. The tip vortices and hub vortices of twin propellers can be resolved using the present approach. At time instant Fig. 26a, vortices separated from propellers are barely disturbed by the aligned rudders, while strong interaction between propellers and rudders can be noticed at the subsequent instants. As for the port side, propeller hub vortices are cut off by the aligned rudder and rudder tip vortices are mixed with the tip vortices of propeller. Unlike the port side behavior, there are two strong separate vortices in the starboard side. One is the hub vortices of propeller and another one is the tip vortices of rudder due to the large attack angle. This phenomenon can also result in the high difference of hydrodynamic loads acting on twin propellers and rudders.

6 Conclusions

In the present work, the in-house CFD solver naoe-FOAM-SJTU is used to directly simulate the performance of ship maneuvering in waves with rotating propellers and turning rudders. Maneuvering control modules are introduced in detail for the standard ship maneuvers, such as course keeping maneuver, zigzag maneuver, and turning circle maneuver. Wave generation modules consisting of inlet boundary wavemaker and relaxation zone wavemaker are also illustrated.

For course keeping maneuver in waves, different heading waves, i.e., head wave, bow quartering wave, and beam wave, are considered to investigate the wave heading effects on the course keeping maneuver. It is concluded that bow quartering wave condition meets the largest heading change and the rudder execution is up to 3.2°. The predicted ship motions and rudder angle agree well with the experimental data. It is proved that the developed course keeping maneuver module is reliable and the present CFD approach can be an alternative tool to predict course keeping maneuver in waves.

For zigzag maneuver in waves, different wave lengths are adopted to investigate the hydrodynamic performance of zigzag maneuver in different waves. Simulated results are compared with the experiment measurements. Predicted overshoot angles and period to complete one zigzag turn show an overall agreement with the measurement data. It is concluded that ship motions increase with the increasing of wave length and the wave-induced motions can be enlarged significantly when wave length is around one ship length.

For turning circle maneuver in waves, the computational cost is the highest with the fact that turning period is very long. Predicted trajectory agrees well with the experiment, while the turning diameter is overestimated by 6.57%. Heave, pitch, and roll motions show obvious wave-induced fluctuations and low frequency maneuvering behavior can also be resolved. In addition, free surface elevation and vortical structures around ship hull, propellers, and rudders are presented to give better understanding of hydrodynamic performance during turning circle maneuver in waves.

Through the simulation of three standard maneuvers, it is proved that the present CFD solver naoe-FOAM-SJTU is reliable and can be used as an alternative tool to predict the hydrodynamic performance of ship maneuvering in waves. Despite the relatively good estimation by the present approach, the RANS method is not accurate enough to resolve the detailed flow separation for ship maneuvering in waves and DES or LES computations are required to improve the prediction accuracy. Therefore, future work will be focused on the prediction accuracy and efficiency of the present solver in simulating ship maneuvering in waves.

References

Araki M, Sadat-Hosseini H, Sanada Y, Tanimoto K, Umeda N, Stern F (2012) Estimating maneuvering coefficients using system identification methods with experimental, system-based, and CFD free-running trial data. Ocean Eng 51:63–84. https://doi.org/10.1016/j.oceaneng.2012.05.001

Berberović E, van Hinsberg N, Jakirlić S, Roisman I, Tropea C (2009) Drop impact onto a liquid layer of finite thickness: dynamics of the cavity evolution. Phys Rev E 79(3):36306. https://doi.org/10.1103/PhysRevE.79.036306

Cao H, Wan DC (2014) Development of multidirectional nonlinear numerical wave tank by naoe-FOAM-SJTU solver. Int J Ocean System Engineering 4(1):52–59. https://doi.org/10.5574/JAROE.2015.1.1.014

Cao H, Wan DC (2015) RANS-VOF solver for solitary wave run-up on a circular cylinder. China Ocean Engineering 29:183–196. https://doi.org/10.1007/s13344-015-0014-2

Cao H, Wan DC (2017) Benchmark computations of wave run-up on single cylinder and four cylinders by naoe-FOAM-SJTU solver. Appl Ocean Res 65:327–337. https://doi.org/10.1016/j.apor.2016.10.011

Carrica PM, Ismail F, Hyman M, Bhushan S, Stern F (2012) Turn and zigzag maneuvers of a surface combatant using a URANS approach with dynamic overset grids. J Mar Sci Technol 18(2):166–181. https://doi.org/10.1007/s00773-012-0196-8

Elshiekh H (2014) Maneuvering characteristics in calm water and regular waves for ONR Tumblehome. Master thesis, The University of IOWA

ITTC (2017) Proposed tasks and structure of the 29th ITTC Technical Committees and Groups. *28th International Towing Tank Conference*. Wuxi, China, 393–408

Jacobsen NG, Fuhrman DR, Fredsøe J (2012) A wave generation toolbox for the open-source CFD library: OpenFoam®. Int J Numer Methods Fluids 70(9):1073–1088. https://doi.org/10.1002/fld.2726

Liu C, Wang J, Wan DC (2018) CFD computation of wave forces and motions of DTC ship in oblique waves. Int J Offshore Polar Engineering 28(2):154–163. https://doi.org/10.17736/ijope.2018.sh21

Menter FR, Kuntz M, Langtry R (2003) Ten years of industrial experience with the SST turbulence model. Turbulence, Heat Mass Transfer 4(1):625–632

Noack RW, Boger DA, Kunz RF, Carrica PM (2009) Suggar++: an improved general overset grid assembly capability. *19th AIAA Conference*, San Antonio, USA, 22–25

Paroka D, Muhammad AH, Asri S (2017) Prediction of ship turning maneuvers in constant wind and regular waves. Int J Technol 8(3):387–397. https://doi.org/10.14716/ijtech.v8i3.3704

Sanada Y, Tanimoto K, Takagi K, Gui L, Toda Y, Stern F (2013) Trajectories for ONR Tumblehome maneuvering in calm water and waves. Ocean Eng 72:45–65. https://doi.org/10.1016/j.oceaneng.2013.06.001

Sanada Y, Elshiekh H, Toda Y, Stern F (2014) Effects of waves on course keeping and maneuvering for surface combatant ONR Tumblehome. 30th Symposium on Naval Hydrodynamics, Hobart, Australia

Seo MG, Kim Y (2011) Numerical analysis on ship maneuvering coupled with ship motion in waves. Ocean Eng 38:1934–1945. https://doi.org/10.1016/j.oceaneng.2011.09.023

Shen Z, Korpus R (2015) Numerical simulations of ship self-propulsion and maneuvering using dynamic overset grids in OpenFOAM. *Tokyo 2015* A Workshop on CFD in Ship Hydrodynamics, Tokyo, Japan

Shen Z, Wan DC (2013) RANS computations of added resistance and motions of a ship in head waves. Int J Offshore Polar Engineering 23(4):264–271

Shen Z, Wan DC (2016) An irregular wave generating approach based on naoe-FOAM-SJTU solver. China Ocean Engineering 30:177–192. https://doi.org/10.1007/s13344-016-0010-1

Shen Z, Ye H, Wan DC (2014) URANS simulations of ship motion responses in long-crest irregular waves. J Hydrodynamics, Ser. B 26(3):436–446. https://doi.org/10.1016/S1001-6058(14)60050-0

Shen Z, Wan DC, Carrica PM (2015) Dynamic overset grids in OpenFOAM with application to KCS self-propulsion and maneuvering. Ocean Eng 108:287–306. https://doi.org/10.1016/j.oceaneng.2015.07.035

Sigmund S, el Moctar O (2017) Numerical and experimental investigation of propulsion in waves. Ocean Eng 144:35–49. https://doi.org/10.1016/j.oceaneng.2017.08.016

Sprenger F, Maron A, Delefortrie G, van Zwijnsvoorde T, Cura-Hochbaum A, Lengwinat A, Papanikolaou A (2017) Experimental studies on seakeeping and maneuverability of ships in adverse weather conditions. J Ship Res 61(3):131–152. https://doi.org/10.5957/JOSR.170002

Subramanian R, Beck RF (2015) A time-domain strip theory approach to maneuvering in a seaway. Ocean Eng 104:107–118. https://doi.org/10.1016/j.oceaneng.2015.04.071

Tezdogan T, Demirel YK, Kellett P, Khorasanchi M, Incecik A, Turan O (2015) Full-scale unsteady RANS CFD simulations of ship behaviour and performance in head seas due to slow steaming. Ocean Eng 97:186–206. https://doi.org/10.1016/j.oceaneng.2015.01.011

Wang J, Wan DC (2016) Investigations of self-propulsion in waves of fully appended ONR Tumblehome model. Appl Math Mech 37(12):1345–1358. https://doi.org/10.21656/1000-0887.370525

Wang J, Liu X, Wan DC (2015) Numerical prediction of free running at model point for ONR Tumblehome using overset grid method, *Tokyo 2015 A Workshop on CFD in Ship Hydrodynamics*, Tokyo, Japan, 383–388

Wang J, Zhao W, Wan DC (2016) Free maneuvering simulation of ONR Tumblehome using overset grid method in naoe-FOAM-SJTU solver. 31th Symposium on Naval Hydrodynamics, Monterey, USA

Wang J, Zou L, Wan DC (2017) CFD simulations of free running ship under course keeping control. Ocean Eng 141:450–464. https://doi.org/10.1016/j.oceaneng.2017.06.052

Wang J, Zou L, Wan DC (2018) Numerical simulations of zigzag maneuver of free running ship in waves by RANS-Overset grid method. Ocean Eng 162:55–79. https://doi.org/10.1016/j.oceaneng.2018.05.021

Ye H, Shen Z, Wan DC (2012) Numerical prediction of added resistance and vertical ship motions in regular head waves. J Mar Sci Appl 11(4):410–416. https://doi.org/10.1007/s11804-012-1150-1

Zha R, Ye H, Shen Z, Wan DC (2014) Numerical study of viscous wave-making resistance of ship navigation in still water. J Mar Sci Appl 13(2):158–166. https://doi.org/10.1007/s11804-014-1248-8

Zha R, Ye H, Shen Z, Wan DC (2015) Numerical computations of resistance of high speed catamaran in calm water. J Hydrodynamics, Ser. B 26(6):930–938. https://doi.org/10.1016/S1001-6058(14)60102-5

Zhang W, Zou Z (2016) Time domain simulations of the wave-induced motions of ships in maneuvering condition. J Mar Sci Technol 21(1):154–166. https://doi.org/10.1007/s00773-015-0340-3